HHS Public Access

Author manuscript

Cell Rep. Author manuscript; available in PMC 2017 February 28.

Published in final edited form as:

Cell Rep. 2016 December 13; 17(11): 2979–2993. doi:10.1016/j.celrep.2016.11.048.

Dual Shp2 and Pten Deficiencies Promote Non-Alcoholic Steatohepatitis and Genesis of Liver Tumor-Initiating Cells

Xiaolin Luo[1], **Rui Liao**[1,3,5], **Kaisa L. Hanley**[2], **Helen He Zhu**[1], **Kirsten N. Malo**[2], **Carolyn Hernandez**[4], **Xufu Wei**[1,5], **Nissi M. Varki**[1], **Nazilla Alderson**[1], **Catherine Chu**[2], **Shuangwei Li**[1], **Jia Fan**[3], **Rohit Loomba**[4], **Shuang-Jian Qiu**[3], and **Gen-Sheng Feng**[1,2,*]

[1]Department of Pathology, School of Medicine, University of California, San Diego, La Jolla, CA 92093, USA

[2]Molecular Biology Section, Division of Biological Sciences, University of California, San Diego, La Jolla, CA 92093, USA

[3]Liver Cancer Institute, Zhongshan Hospital, Fudan University, Shanghai 200032, China

[4]NAFLD Research Center, Department of Medicine, University of California, San Diego, La Jolla, CA 92093, USA

[5]Department of Hepatobiliary Surgery, The First Affiliated Hospital, Chongqing Medical University, Chongqing 40016, China

SUMMARY

The complexity of liver tumorigenesis is underscored by the recently observed anti-oncogenic effects of oncoproteins, although the mechanisms are unclear. *Shp2/Ptpn11* is a proto-oncogene in hematopoietic cells, and antagonizes the effect of tumor suppressor *Pten* in leukemogenesis. In contrast, we show here cooperative functions of Shp2 and Pten in suppressing hepatocarcinogenesis. Ablating both Shp2 and Pten in hepatocytes induced early-onset non-alcoholic steatohepatitis (NASH), and promoted genesis of liver tumor-initiating cells likely due to augmented cJun expression/activation, and elevated ROS and inflammation in the hepatic microenvironment. Inhibiting cJun partially suppressed NASH-driven liver tumorigenesis without

[*]***Corresponding Author and Lead Contact***: Dr. Gen-Sheng Feng (gfeng@ucsd.edu).

SUPPLEMENTAL INFORMATION

Supplemental Information includes seven figures and seven tables.

AUTHOR CONTRIBUTIONS

X.L. and G.-S.F. conceived and designed the project, analyzed the data, and wrote the paper. G.-S.F. provided the reagents. X.L. designed and performed most of the experiments. X.W. analyzed the expression of SHP2 and PTEN in HCC patients with IHC and Western blot. R.L., S.Q. and J.F. provided human HCC TMA samples. C.H. and L.R. provided human NAFL and NASH liver sections. N.M.V. helped pathology analysis. X.L. and N.A. purified the AAV8 viruses. S.L. and H.H.Z. helped analyze the data. K.L.H. and K.N.M. helped with the human HCC TMA staining and data analysis. K.L.H., C.C., N.A. and K.N.M. helped with genotyping, immunoblotting and immunostaining.

ACCESSION NUMBERS

The microarray data for liver samples of 2-month-old mice have been deposited in the Gene Expression Omnibus (GEO) under the accession number GSE74732.

improving NASH. SHP2 and PTEN deficiencies were detected in liver cancer patients with poor prognosis. These data depict a mechanism of hepato-oncogenesis and suggest a potential therapeutic strategy.

Abstract

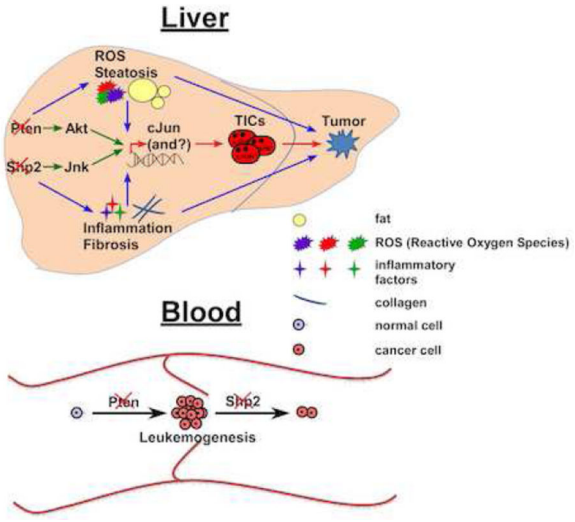

INTRODUCTION

Primary liver cancer, mainly hepatocellular carcinoma (HCC), has become the 2nd leading cause of cancer-related death worldwide (Theise, 2014) . Although its etiology is strongly associated with hepatitis B or C virus (HBV or HCV) infections in Asian and African countries, the rapidly rising incidences in the Western world are linked to obesity, alcohol abuse, non-alcoholic fatty liver disease (NAFLD) or steatohepatitis (NASH). NASH is one major manifestation of metabolic disorders, which trigger hepatic injuries, inflammation, fibrosis and carcinogenesis (Lade et al., 2013; Michelotti et al., 2013).

Genetic analyses of human HCC samples have detected aberrant activation of classical oncogenic signaling pathways, such as MET, Wnt/β-catenin, NF-κB, and JNK (Kaposi-Novak et al., 2006; Pilati et al., 2014; Zucman-Rossi et al., 2015). Deficient expression or inactivating mutations were also detected in classical tumor suppressor genes, such as *p53*, *RB*, *p21* and *p27* in human liver cancers (Zucman-Rossi et al., 2015). Pten (phosphatase and tensin homologue deleted from chromosome 10), a lipid phosphatase for phosphatidylinositol 3, 4, 5-trisphosphate, is a classical tumor suppressor that counteracts PI3K signaling (Cantley, 2002; Song et al., 2012; Worby and Dixon, 2014). *Pten* deficiency or mutations were detected in various types of human cancer, including HCC (Chalhoub and Baker, 2009), and targeted *Pten* deletion in hepatocytes led to spontaneous development of HCC or ICC (intrahepatic cholangiocarcinoma) in mice (Galicia et al., 2010; Horie et al., 2004; Kenerson et al., 2013).

The above clinical and experimental data argue that liver tumorigenesis shares common mechanisms, i.e. over-activation of proto-oncogenes and/or loss/inactivation of tumor

suppressors resulting in neoplastic cell proliferation. Accordingly, great efforts have been devoted to the development of pharmaceutical compounds that disrupt the classical oncogenic pathways for liver cancer therapy, with Sorafenib, a multikinase inhibitor, as the most widely used drug (Llovet et al., 2008). Unfortunately, Sorafenib and other similar oncoprotein inhibitors have achieved very little therapeutic benefit for HCC patients (Llovet et al., 2008). The systematic failure in the "mechanism-based" HCC therapy is evidently due to inadequate understanding of the complexity in hepatocarcinogenesis. One interesting finding made by several groups recently is the unanticipated anti-oncogenic effect of classical oncoproteins (Feng, 2012). Deletion of *Met*, *Egfr*, *ctnnb1* or *Ikkβ* in hepatocytes surprisingly enhanced HCC development in mice treated with a chemical carcinogen diethylnitrosamine, DEN (Feng, 2012; Lanaya et al., 2014; Maeda et al., 2005; Takami et al., 2007; Zhang et al., 2010). These data may explain why inhibiting classical oncogenic pathways achieved little therapeutic effect for HCC patients, and also unlock the previously unrecognized complexity of liver tumorigenesis, which urgently needs elucidation.

Shp2/Ptpn11 is the first identified oncogenic tyrosine phosphatase, with dominantly activating mutations detected in several types of leukemia (Chan and Feng, 2007), and Shp2 positively regulates Ras-Erk signaling (Lai et al., 2004; Neel et al., 2003). Indeed, ablating Shp2 abrogates myeloproliferative neoplasm induced by Pten loss, indicating opposing effects between the two molecules in myeloid cells (Zhu et al., 2015). However, in contrast to its pro-leukemogenic effect, deleting *Shp2* in hepatocytes triggered hepatocellular adenoma (HCA) in aged mice and also enhanced DEN-induced HCC development (Bard-Chapeau et al., 2011). Nevertheless, the concept that these oncoproteins act as tumor suppressors in the liver has not been well accepted, due to concerns on the relevance of DEN-induced animal models to HCC patients. We choose to dissect the anti-oncogenic role of Shp2 in the liver by determining its functional interaction with a classical tumor suppressor Pten.

RESULTS

Simultaneous Deletion of *Shp2* and *Pten* Cooperatively Promotes Liver Tumorigenesis

We generated a hepatocyte-specific *Pten* and *Shp2* double knockout (*DKO*) mouse line ($Pten^{fl/fl}$:$Shp2^{fl/fl}$:*Alb-Cre*$^{+}$), by crossing $Shp2^{fl/fl}$ (Zhang et al., 2004) and $Pten^{fl/fl}$ (Lesche et al., 2002) mice with *Albumin-Cre* transgenic mice. In this study, we performed comparative phenotypic analysis of *DKO with SKO* ($Shp2^{hep-/-}$, or $Shp2^{fl/fl}$:*Alb-Cre*$^{+}$), *PKO* ($Pten^{hep-/-}$, or $Pten2^{fl/fl}$:*Alb-Cre*$^{+}$) and *WT* ($Pten2^{fl/fl}$:$Shp2^{fl/fl}$:*Alb-Cre*$^{-}$) mice. Deletion of either *Shp2* or *Pten* alone did not cause liver tumors until late stages (Figure 1A–B). However, 80% of *DKO* mice spontaneously developed liver tumors in 5 months, and the tumor incidences reached 100% at 7 months of age. By evaluating tumor numbers, sizes (maximal tumor diameter), and liver to body weight ratios, we found that ablating both *Shp2* and *Pten* triggered more severe liver tumorigenesis than deleting either gene alone at all time points examined.

Pathological examination of 60 *WT* mice in total revealed no hepatic tumor by 18 months of age (Table S1). We detected HCA in 2/6 *SKO* mice at 12 months and in 6/7 of the mice at 18 months, consistent with previous observation (Bard-Chapeau et al., 2011). By examining 12

PKO mice at 7 months, we detected ICC in one and HCA in three, with no tumor nodules observed before 7 months. Tumor incidences rose up to 100% (11/11) in *PKO* mice at the age of 12 months, and all tumors were either HCA or ICC, with no HCC observed. At 16 months of age, 3/7 *PKO* animals developed HCC. Notably, deleting both *Shp2* and *Pten* dramatically accelerated tumor initiation and malignant transition. We detected HCA in 6/9 and HCC in 2/9 *DKO* mice examined at 4–5 months, and 6/10 *DKO* mice had HCC at 7 months. We also observed mixed ICC/HCC tumors in *DKO* mice, and 3 *DKO* mice with HCC exhibited lung metastasis at 12 months (Figure 1E).

Histological analysis showed similar pathological features for tumors from *PKO* and *DKO* livers (Figure 1C–D), and HCAs in both *PKO* and *DKO* showed tumor cells with large lipid droplets in the cytoplasm and the nucleus against the cell membrane. HCCs exhibited a trabecular pattern and had less lipids in cells and stained positive for HepPar-1. ICCs displayed well-differentiated tubules lined with one or multiple layers of cuboidal epithelial cells that were CK-19-positive. Tumors with mixed HCC/ICC phenotype stained partly positive for HepPar-1 and CK-19. PCR analysis of genomic DNA and immunoblotting of proteins confirmed efficient deletion of *Shp2* and/or *Pten* in both tumor and non-tumor tissues in respective animals (Figure 1F). Immunoblotting also detected markedly elevated levels of Cyclin D1 and PCNA in both *PKO* and *DKO* tumors relative to tumor-surrounding tissues, with no significant difference observed for c-Myc and β-catenin expression among the four groups of mice.

Combined Shp2 and Pten Deficiencies in Hepatocytes Trigger Early-Onset NASH

PKO mice developed hepatomegaly and NAFLD at 2 months, consistent with previous reports (Horie et al., 2004; Stiles et al., 2004), but *DKO* animals had even more severely enlarged livers at the same age and their liver to body weight ratios increased significantly compared to the other three groups (Figure S1A–B). Quantification of Oil-Red-O staining and triglyceride levels showed comparable fat deposition in *PKO* and *DKO* mice; histological analysis revealed hepatocytes with fat pellets in both peri-central and peri-portal areas in *DKO*, while steatosis was detected only in the peri-central area in *PKO* mice (Figure 2A, Figure S1C). Free fatty acids (FFA) were elevated significantly in both *PKO* and *DKO* livers but not in sera (Figure S1D). Conversely, cholesterol increased significantly in both *PKO* and *DKO* sera but not in their livers (Figure S1E). These data demonstrate that both *PKO* and *DKO* mice developed hepatosteatosis, and that additional *Shp2* ablation modestly aggravates the phenotype induced by Pten loss.

To probe the underlying mechanism, we profiled the expression of key genes involved in lipid metabolism and gluconeogenesis in 2-month-old livers (Figure 2B). *Pparg* expression was induced more robustly in livers of *DKO* and *PKO* than *WT* and *SKO*, and *Cd36*, a *Pparg* downstream target that regulates lipid uptake and transport, was significantly upregulated in *PKO* and even more in *DKO*, suggesting increased lipid uptake in the livers. Increase of *Fas* and *Scid1*, encoding two critical lipogenic enzymes, was also detected in *DKO* and *PKO*, suggesting enhanced *de novo* lipid synthesis. *Hsl* and *Atgl*, coding for rate-limiting enzymes in lipolysis, were modestly or significantly lower in *DKO* or *PKO* livers, providing evidence of impaired hepatic lipolysis. Of special interest, we found that the expression of genes

involved in lipid oxidation, including *Ppara*, *Aco*, *Lcad* and *Mcad* and genes involved in gluconeogenesis, such as *G6p* and *Pepck*, were significantly attenuated in *DKO* but not in *PKO* liver. We also examined the expression profiles of the same set of genes in 1-month-old livers, and obtained consistent results in 1- and 2- month-old mice of the four genotypes (Figure S1F). These data suggest that the severe hepatosteatosis phenotype in *DKO* was caused collectively by metabolic changes in lipogenesis, uptake, lipolysis, oxidation and gluconeogenesis. After feeding the mice high-fat diet (HFD) for one month, we observed significantly elevated triglyceride levels in *DKO* mice on HFD relative to normal chow diet, but not in *WT* controls (Figure S1G), suggesting increased susceptibility of *DKO* mice to HFD-induced hepatic steatosis.

Histological examination revealed severe infiltration of inflammatory cells in portal triads with extension to the parenchyma in *DKO* liver (Figure 3A), and mild inflammation was observed in *SKO*, but not in *PKO*, consistent with previous reports (Bard-Chapeau et al., 2011; Horie et al., 2004). Immunostaining showed that Kupffer cells ($F4/80^+$), neutrophils ($Ly6G^+$) and T cells ($CD3^+$), but not B cells ($B220^+$), were significantly increased in *DKO* liver (Figure 3A). Marked increase in the spleen to body weight ratios was detected in *SKO*, and the ratios were even more elevated in *DKO* mice, indicating enhanced systematic inflammatory and immune responses (Figure 3B). Consistently, microarray and qRT-PCR analyses demonstrated that many inflammatory factors and related receptors, such as *Tnfa*, *Fgf21*, *Pdgfa*, *Pdgfc*, *Ccl21a* and *Cx3cl1*, were more dramatically induced in *DKO* than the other three groups (Figure 3C, Figure S2D).

Moreover, *DKO* livers showed the most severe fibrosis, as evaluated by Picro-Sirius Red and Masson's Trichrome staining (Figure 3D). Activated hepatic stellate cells, the major source of collagen, were largely expanded in *DKO*, as determined by α-SMA staining (Figure 3D). Tunel staining showed more hepatocyte apoptosis in *DKO* livers (Figure 3E), accompanied by drastic increase in serum ALT levels (Figure 3F), further indicating more severe hepatic injuries. In addition, ballooning hepatocytes and Mallory-Denk bodies (MDB) were detected in *DKO* livers (Figure 3G, H). PCNA and Ki67 staining showed more active hepatocyte proliferation (Figure 3E). Consistent to our previous report (Li et al., 2014), hepatic bile acid levels were elevated in *SKO*, but the increase was compromised by additional *Pten* deletion in *DKO* livers (Figure S2A). Accordingly, Cyp7a1, a key enzyme for bile acid synthesis, was induced in *SKO* but this induction was blunted in *DKO* livers (Figure S2B–C). We further analyzed the toxicogenomic changes using IPA-Tox® with the microarray data. Dual deletion of *Shp2* and *Pten* induced changes related to NASH, such as liver fibrosis, steatosis, cell death and proliferation, inflammation, hepatitis and enlargement, as shown at the top of the list (Figure S2E). In conclusion, young *DKO* animals exhibited typical NASH signs, resembling a subset of human NASH patients (Chalasani et al., 2012).

Next, we deleted Shp2 and Pten acutely in adult mice ($Shp2^{fl/fl}$:$Pten^{fl/fl}$) with adeno-associated virus expressing Cre (AAV-Cre), with AAV-GFP as a control, and then subjected the mice to CCl_4 treatment. Immunoblotting showed that Shp2 and Pten were efficiently removed by AAV-Cre infection (Figure S2F). CCl_4 treatment led to mild liver damage in control mice but caused severe damage in livers with both Shp2 and Pten deleted, as revealed by increased fibrosis and inflammation, serum ALT, and spleen to body weight

ratios (Figure S2G–J). These results suggest a cooperative role of Shp2 and Pten in protection against hepatic injuries.

The Liver TIC Population Expands in Young *DKO* mice

The earlier detection of tumor nodules in *DKO* than *PKO* mice suggests that additional *Shp2* deletion accelerates the initiation and/or progression of liver tumorigenesis triggered by *Pten* loss. To sort out these possibilities, we evaluated the expression of biomarkers for liver TICs in young mice at 2 months of age, when no tumor nodules were visible. qRT-PCR detected significantly elevated mRNA levels of *EpCam*, *Ck19*, *Prominin1*, *Cd44* and *Ly6D*, but not *Afp*, in *DKO* livers (Figure 4A). Consistently, immunostaining detected increased number of cells positive for EpCAM, Ly6D, CD44, CK19 and CD44v6 in *DKO* liver sections (Figure 4B), and $A6^+$ oval cells were also increased (Figure 4B). Although *Sox9* mRNA was not changed (Figure 4A), the $SOX9^+$ cell population was dramatically expanded in *DKO* liver (Figure 4B). Of note, cells positive for EpCAM, CK19, CD44v6 or SOX9 were mainly located in the portal triad area, while those stained with CD44 or Ly6D were scattered in the liver, suggesting heterogeneity of the TIC population. Furthermore, co-immunostaining for CD44v6/SOX9 and EpCAM/SOX9 consistently detected the expansion of TICs in *DKO* livers (Figure 4C). We then examined tumors and surrounding tissues in 12-month-old *DKO* mice, using SOX9 as a marker (Figure 4D). Very few $SOX9^+$ cells were detected in non-tumor tissues or HCAs, but extensive staining of SOX9 was observed in ICCs, HCCs, mixed ICC/HCC tumors and lung-metastasized nodules.

Following examination of physical markers, we performed functional analysis of liver TICs in young mice, before detection of visible tumor nodules. We isolated hepatocytes from 2–3 month-old mouse livers and injected 1.2×10^5 viable cells intra-splenically into 21-day-old *MUP-uPA* transgenic mice, as described previously (He et al., 2013). By examining liver tumorigenesis in recipients after 5 months, we found no tumors in mice transplanted with *WT* or *SKO* hepatocytes, and tiny tumors in 2/7 recipients for *PKO* hepatocytes. In contrast, 7/8 mice that received *DKO* hepatocytes had tumors and their tumor burdens were much heavier (Figure 4E, F). Pathological examination detected two types of tumor, HCC and HCC/ICC mixture in recipients for *DKO* hepatocytes, and both types of tumor contained $SOX9^+$ cells (Figure S3A). PCR analysis of genomic DNA and immunoblotting of proteins extracted from these tumors confirmed deletion of *Shp2* and *Pten*, proving that these tumors originated from transplanted donor cells (Figure 4G). Tumor nodules were even detected in the lung of two recipients of *DKO* hepatocytes (Figure 4H), which were $SOX9^+$ and histologically similar to HCCs (Figure S3B). Thus, concurrent Shp2 and Pten deletion induced earlier expansion of a functional liver TIC population.

cJun is Upregulated in Shp2/Pten-deficient Liver

We investigated the molecular mechanisms that drive the expansion of TICs in *DKO* liver. Global gene expression profiling by cDNA microarray analysis of 2-month-old liver samples revealed upregulation of several proto-oncogenes in *DKO* mice (Table S2). In particular, on top of the list is *cJun*, a proto-oncogene that plays a critical role in hepatogenesis, liver regeneration, tumor initiation and progression (Eferl and Wagner, 2003; Ransone and Verma, 1990).

cJun mRNA increase detected in the microarray analysis was confirmed by qRT-PCR (Figure 5A). Immunoblotting showed that both the protein amount and phosphorylation of cJun were elevated in *DKO* livers (Figure 5B), indicating higher expression and activity. Consistently, immunostaining detected more $cJun^+$ cells in DKO liver sections (Figure 5C). cJun upregulation could be stimulated by altered intracellular signaling and hepatic microenvironment. Indeed, both liver and systematic inflammations were significantly enhanced in *DKO* animals (Figure 3A–B). Multiple cytokines, growth factors and related receptors were upregulated in *DKO* livers (Figure 3C, Figure S2D). We examined reactive oxygen species (ROS), and observed more extensive staining with dihydroethidine (DHE) for superoxide anions, and with 4-HNE for lipid peroxidation aggregates in *DKO* livers (Figure 5D). Interestingly, the periportal areas, where more TICs were found, showed increased staining for the ROS markers. Consistently, we detected more severe DNA damage in *DKO* livers, by staining with pH2AX antibody (Figure 5D). qRT-PCR analysis showed lower expression of H_2O_2 scavengers *Gpx1*, *Gpx2* and *Catalase* and antioxidant enzymes *Sod1*, *Sod2*, *Gsta1*, *Gst* and *Gstp1* in *SKO* and *DKO* livers (Figure 5E).

To evaluate a possible microenvironmental effect on cJun upregulation, we treated *DKO* mice with lenalidomide, an analogue of thalidomide that acts to inhibit expression of cytokines, such as TNFα (Zhu et al., 2014). Increased TNFα was detected in *DKO* livers (Figure S2D), and lenalidomide treatment downregulated TNFα expression (Figure 5F). Consistently, the mRNA, protein and phosphorylation levels of cJun also decreased (Figure 5F–G), accompanied by reduced TIC population (Figure S4). These results suggest that the inflammatory factors, especially TNFα, contributed to cJun upregulation in *DKO* livers. However, lenalidomide treatment did not suppress cJun to the basal level, suggesting that intracellular signaling altered by Shp2 and Pten deletion may also play a role in cJun upregulation. As expected, p-Akt levels were markedly elevated by Pten loss, and this effect was modestly attenuated by additional Shp2 deletion (Figure 5H). Decreased p-Erk signals were observed in *SKO* and *DKO* livers, relative to WT and *PKO*, reinforcing a positive role of Shp2 in Erk activation (Lai et al., 2004; Neel et al., 2003), without an obvious effect on p38 activity. In contrast, p-Jnk signals were robustly induced by ablating Shp2 in *SKO* and *DKO* livers (Figure 5H), supporting our previous data indicating a negative role of Shp2 in Jnk activation (Bard-Chapeau et al., 2006; Shi et al., 1998). pY-Stat3 was elevated in *SKO* livers as previously reported (Bard-Chapeau et al., 2011), but this effect was compromised by additional Pten deletion in *DKO* livers (Figure 5H). As it has been well documented that Akt can activate cJun/AP-1 (Cross et al., 1995; Gotschel et al., 2008; Li et al., 2004; Peloponese and Jeang, 2006), we believe that the excessive cJun expression and activation in DKO liver are likely contributed by simultaneous over-activation of Akt and Jnk induced by removal of Pten and Shp2, respectively, together with the elevated inflammation and ROS levels in the hepatic microenvironment (Figure 7E).

Inhibition of cJun Suppresses Liver Tumorigenesis but not NASH

We investigated the potential role of cJun in TIC expansion by examining its expression profile. Co-immunostaining showed that almost all $EpCAM^+$ or $A6^+$ cells were also positive for cJun in 2-month-old *DKO* liver (Figure 6A), confirming cJun induction in TICs. In cultured HepG2 cells, the subpopulation with higher EpCAM also exhibited increased cJun

expression (Figure 6B). We then determined the effect of cJun inhibition by expressing TAM67, a dominant-negative form of cJun acting to sequester cJun into low activity complexes (Brown et al., 1993; Shimizu et al., 2008). In an in vitro sphere-forming assay (He et al., 2010), expressing TAM67 in HepG2 cells significantly decreased the sphere numbers, compared to the control (Figure 6C). We then introduced TAM67 into 1-month-old *SKO*, *PKO* and *DKO* liver using AAV8 virus, and evaluated TIC expansion and tumorigenesis. qRT-PCR analysis of the downstream targets of *cJun*, *cFos*, *JunB* and *JunD* (Eferl and Wagner, 2003) showed that TAM67 potently suppressed *cJun* and slightly reduced *cFos*, without obvious effect on *JunB* or *JunD* in *DKO* livers (Figure S5A). After one month of infection, the TIC population was severely suppressed in *DKO* mice while only slightly decreased in *SKO* and *PKO* mice (Figure S5B–C). The expression of TAM67 was high at 1 month after infection, but barely detectable after 6 months (Figure S5D). TAM67 delivery significantly suppressed the tumor number and moderately reduced tumor sizes, without affecting tumor incidences and liver weights, compared to GFP controls (Figure 6D–E). qRT-PCR and immunostaining also showed suppression of TIC markers including EpCAM, CK19, Ly6D, CD44 and SOX9 in *DKO* livers by expressing TAM67 (Figure 6F–G). Notably, the NASH symptoms were not improved by inhibiting cJun in *DKO* livers (Figure S5E–G), which indicates its direct effect on liver tumorigenesis by inhibiting TIC expansion, independent of steatohepatitis. A previous report showed that cJun enhanced DEN-induced liver tumorigenesis by inducing Survivin (Min et al., 2012). By co-immunostaining, we detected co-localization of Survivin and EpCAM in *DKO* liver sections (Figure 6H), and expressing TAM67 decreased Survivin^{+} cells in *DKO* liver (Figure S5H), supporting a role of Survivin downstream of cJun.

SHP2 and PTEN Deficiencies Correlate with Poor Prognosis in HCC Patients

To assess the clinical significance of SHP2 and PTEN deficiency, we performed immunostaining for SHP2 and PTEN on a tissue microarray (TMA) with 350 self-paired human HCC specimens (Table S3–5). Both SHP2 and PTEN showed cytoplasmic staining, and scores of 0–3 were given, with 0 indicating no or very weak, 1 for weak, 2 for medium and 3 for strong staining (Figure S6B). We compared SHP2 or PTEN expression in each tumor with the paired tumor-surrounding tissue. In total, we identified 106, 113 and 131 pairs of specimens with SHP2 expression higher, comparable and lower in tumors than surrounding tissues, respectively, while the corresponding numbers for PTEN were 58, 86 and 191, respectively (Figure 7A). Similar results of variable SHP2 and PTEN expression were obtained by examining a different TMA that contained 45 pairs of human HCC tumors and surrounding tissues purchased from US Biomax (Figure S6A).

We then assessed the prognostic value of SHP2 and PTEN expression, and found that lower expression of SHP2 or PTEN alone in tumors was significantly associated with shorter overall and disease-free survival time (Figure 7B, C). Deficient SHP2 expression in tumors also correlated with larger tumor sizes and higher serum AFP levels (Table S3). To determine the prognostic value of combined SHP2 and PTEN deficiencies, we further classified the 335 HCC patients into four groups: I, low expression of both SHP2 and PTEN; II, low SHP2 but high PTEN expression; III, high SHP2 but low PTEN expression; and IV, high expression of both SHP2 and PTEN. SHP2^{L} or PTEN^{L} included SHP2 or PTEN

staining scores of 0–1, and $SHP2^{H}$ or $PTEN^{H}$ were for staining scores of 1–3 (excluding 1). The group I patients with low expression of both showed significantly shorter overall and disease-free survival time (Figure 7D). Furthermore, the tumor sizes and AFP amounts of group I patients were significantly larger and higher, respectively (Table S5). These data argue for the clinical relevance of SHP2 and PTEN deficiencies in human HCC development and prognosis.

We further examined SHP2 and PTEN expression in liver samples of patients at NAFLD, NASH12 or NASH34 stages (Table S6). Immunostaining detected variable levels of SHP2 and PTEN expression; the SHP2 expression correlated inversely with the advancing disease stages while PTEN expression did not show significant difference among these groups (Figure S7A–B). However, two recent papers reported inverse correlation of PTEN expression in hepatocytes with NAFLD progression (He et al., 2016; Sanchez-Pareja et al., 2016). Notably, the expansion of $SOX9^{+}$ cells was associated with the advancement of NAFLD to NASH stages (Figure S7C). By examining SOX9 expression in the TMA with 335 HCC specimens, we identified 42 samples with low SHP2 and PTEN expression and also with large number of $SOX9^{+}$ cells (Figure S7D). Together, these results suggest involvement of SHP2 and PTEN deficiencies in human pathogenesis of NASH-driven HCC.

DISCUSSION

The concerted actions of Shp2 and Pten in suppressing liver tumorigenesis is astonishing, because we have just reported mutually neutralizing effects of concurrent Shp2 and Pten deletion in myeloproliferation and leukemogenesis (Zhu et al., 2015). The hepatic phenotype of *DKO* mice unequivocally defines a tumor-inhibitory role of Shp2 in the liver, by working in concert with a classical tumor suppressor Pten in hepatocytes. A model to illustrate the underlying mechanisms is presented in Figure 7E. Pten loss leads to Akt over-activation and Shp2 deficiency promotes Jnk upregulation, resulting in increased cJun expression and activation. Ablating Pten and Shp2 also leads to elevated ROS, inflammation and steatohepatitis, driving earlier genesis of TICs and enhanced tumorigenesis.

NAFLD has become a serious public health problem worldwide (Michelotti et al., 2013), and NASH, an advanced state of NAFLD, is characterized by hepatic steatosis, injury and inflammation with or without fibrosis (Chalasani et al., 2012). The pathogenesis from NAFLD to NASH likely initiates with metabolic disorders that cause hepatosteatosis, and then progresses to steatohepatitis, due to oxidative stress and inflammation etc. *Pten* deficiency in hepatocytes induced excessive activation of the PI3K/AKT pathway, increased lipogenesis and reduced lipolysis, resulting in hepatic lipid accumulation and injuries. Additional removal of Shp2 did not dramatically exacerbate the fatty liver phenotype but did cause liver inflammation, damage and fibrosis at young age. Thus, combined Pten and Shp2 deficiency induced NASH immediately without even a NAFLD stage, by simultaneously triggering multiple hits in *DKO* mice.

The molecular mechanisms underlying NASH-induced liver carcinogenesis remain to be elucidated, and several mouse models have recently been developed to tackle this problem. Mice fed with CDE (choline deficiency and ethionine supplemented) diet developed fatty

liver in 14 days, and long-term (19 months) feeding of this diet caused HCC (Aharoni-Simon et al., 2011). However, CDE diet is highly toxic and led to high mortality with long-term application, which limits its use as a NASH-HCC model (Yoshida et al., 1993). Mice treated with DEN and fed with HFD developed HCC at 50 weeks (Park et al., 2010), but it is unclear whether these mice had NASH symptoms at young age. Feeding MUP-uPA transgenic mice with HFD induced signs of NASH at young age and HCC development at late stages (Nakagawa et al., 2014). Another NASH-HCC model was established by feeding mice with a choline-deficient HFD, which recapitulated human NASH characteristics, and 25% of the mice developed HCC after one year of feeding (Wolf et al., 2014). By deleting Shp2 and Pten, we have established a NASH-HCC model, in which HCC develops spontaneously in 7 months, without DEN treatment. The DKO mice, recapitulating many features of NASH patients, may represent a useful animal model for extensive search of molecular signals that drive NASH to HCC.

The earlier genesis of TICs evidently contributed to the severe phenotype of liver tumorigenesis in the *DKO* mouse. This conclusion is not only based on detection of physical markers but also relies on the functional determination of TICs in vivo. Intra-splenic transplantation of hepatocytes isolated from 2-month-old *DKO* liver into *MUP-uPA* mice caused growth of numerous tumor nodules in the liver recipients. We believe that the early-onset NASH is a critical factor for TIC activation and expansion. Excessive lipid accumulation in hepatocytes is toxic and boosts ROS levels, causing genome instability and cell death. These damages could switch on the innate immune system, represented by expansion of Kupffer cells, infiltration of inflammatory cells, and secretion of cytokines and chemokines. Moreover, liver injuries could also activate HSCs to synthesize and secrete more collagens that induce fibrosis. Together, these hepatic micro-environmental factors promoted TIC activation.

One molecular link between the micro-environment and activating TICs is possibly cJun, which was potently induced and activated by inflammatory factors and ROS in *DKO* liver combined with augmented Akt and Jnk signaling (Figure 7E). cJun expression overlapped with progenitor cell markers EpCAM and A6, and inhibiting cJun with a dominant negative form TAM67 in HepG2 cells impaired the self-renewal capacity in vitro. Expression of TAM67 in *DKO* liver also suppressed TIC expansion and tumorigenesis in vivo, even though the NASH symptoms were not improved. Therefore, cJun inhibition uncouples the micro-environmental signals from TIC activation. Of note, cJun is not likely the sole link between these processes and other mechanisms may be involved in over-activation of TICs.

By screening two independent tissue microarrays of human liver cancer (mainly HCC) samples, we detected deficient expression of SHP2 and/or PTEN in tumors relative to the surrounding tissues. Strikingly, the survival curves indicated poor prognosis of the patients with SHP2 and PTEN deficiencies. In a recent report (Jiang et al., 2012), the authors screened 333 human HCC samples and detected significantly decreased expression of SHP2 in 235 tumors in correlation with poor prognosis. Analysis of a different cohort of HCC samples detected over-expression of SHP2 in association with HCC progression and poor prognosis (Han et al., 2015). The complexity of big patients' data is expected and likely

represents the diverse age, sex, and disease backgrounds, compared to the mouse models with clean genetic background and targeted deletion of specific genes.

In contrast to the anti-tumorigenic role of Shp2 described here, a recent report indicated that inhibiting Shp2 by shRNA or chemical compound selectively suppressed proliferation of cancer cells driven by receptor tyrosine kinases (Chen et al., 2016). Although hyperactivation of Akt is frequently detected in human cancers and is therefore a therapeutic target, hepatic deletion of Akt1 in $Akt2^{-/-}$ mice surprisingly triggered spontaneous HCC development (Wang et al., 2016). Given the bidirectional roles of these signaling molecules in liver tumorigenesis and the disappointing therapeutic effect of Sorafenib, we propose here that targeting further downstream and signal-culminating molecules may be a more efficient pharmaceutical means for treatment of liver cancer.

EXPERIMENTAL PROCEDURES

Animal Protocols

Hepatocyte-specific *Shp2* KO mice (*SKO, $Shp2^{hep-/-}$*) were generated and characterized as described previously (Bard-Chapeau et al., 2011; Bard-Chapeau et al., 2006; Li et al., 2014). *$Pten^{flox/flox}$* (Lesche et al., 2002) mice were bred with *Albumin-Cre^{+}* transgenic mice to generate hepatocyte-specific *Pten* KO mice (*PKO*) and crossed with *$Shp2^{flox/flox}$* to produce *Shp2* and *Pten* double knockout (*DKO*) animals. *MUP-uPA* transgenic mice were kindly provided by M Karin, UCSD. The animal protocols (s09108) for all procedures were approved by the UCSD Institutional Animal Care and Use Committee (IACUC). Collection of mouse liver and other samples was done at the same time during the day. qPCR, H&E staining, immunostaining, immunoblotting, and FACS sorting were performed following standard procedures, and ImageJ was used to quantify staining data. PCR primers and antibodies are listed in Table S7. Primary hepatocytes were isolated from 2–3 month-old mice as described previously (Bard-Chapeau et al., 2011). Mice were fed with HFD (Research Diets, New Brunswick, NJ, Cat.No. D12451). Mice were injected I.P. with olive oil or CCl4 (1 ml/kg body weight, Sigma-Aldrich, Cat.No.289116) twice a week for 4 weeks. Mice were oral gavaged with lenalidomide (50 mg/kg per day for five days, Selleck Chemicals, Huston, TX, Cat.No.S1029). Intrasplenic transplantation was performed as described previously (He et al., 2013; He et al., 2010). Briefly, 1.2×10^5 viable hepatocytes in 30 μl PBS were transplanted into 21-day-old *MUP-uPA* mice via intrasplenic injection with a 26-G needle. Five months after transplantation, mice were sacrificed for examination of liver tumors. Liver and/or serum triglycerides, bile acids, cholesterol and FFA levels were determined with commercial kits (triglyceride and cholesterol: Sekisui Diagnostics, Kent, UK, Cat.No. 236–60,234–60; bile acid: Cat.No. DZ042A–K, Diazyme Laboratories, Poway, CA; FFA: Cayman Chemical, Ann Arbor, Michigan, Cat.No. 700310). Oil-red-O, Picro-sirius red and Masson's trichrome staining were performed with commercial kits (American MasterTech, Lodi, CA, Cat.Nos.STORO, STPSR and KTMTR).

Microarray, heatmap and IPA analysis of Gene Expression

Microarray analysis of RNAs was performed as previously described (Li et al., 2014). Heatmap was generated using GENE-E (http://www.broadinstitute.org/cancer/software/

GENE-E/index.html) with microarray data, which was also analyzed with Ingenuity IPA (http://www.ingenuity.com/products/ipa).

Cell Culture and Hepatosphere Forming Assay

HepG2 (ATCC HB-8065) cells were cultured following ATCC instructions. Hepatosphere forming assay was performed as previously described (He et al., 2010), with modification. Briefly, 5000 cells were seeded in 6-well ultra-low attachment plate (Corning 3471) with sphere formation medium (DMEM/F12 medium, 20 ng/ml of EGF, 20 ng/ml of bFGF, 1% B27 supplement). Spheres were counted under microscope after 7-day culture.

DHE Staining

DHE staining was performed as previously described (Maeda et al., 2005). Briefly, frozen liver sections were stained with 2 μM dihydroethidine hydrochloride (Life Technologies, Carlsbad, CA, Cat.No.D11347) for 30 min at 37 °C.

Generation and Administration of Recombinant AAV8 Viruses

The adeno-associated virus (AAV) expression system (Stratagene, La Jolla, CA, Cat.No. 240071, 240074) was used to produce AAV-green fluorescent protein (GFP) and AAV-TAM67 virus, with pAAV8-RC replacing pAAV-RC. Primers used for AAV-TAM67 construction and virus titration are listed in Table S7. AAV viruses (~ 4×10^{11} GV/mouse) were diluted in PBS and injected through the tail vein. AAV-Cre virus was purchased from the Vector Core of University of Pennsylvania.

Human Materials

All archival specimens for human HCC Tissue Microarray were obtained from 350 consecutive patients after surgical resection in 2007 with pathologically confirmed HCC (Table S3–5). The experimental protocols described in this study complied with the Ethics Review Committee of Zhongshan Hospital, Shanghai, China, and every patient provided written informed consent before enrollment. TMAs were constructed as previously described (Liao et al., 2012). All patients were monitored postoperatively until January 2012. All the IHC staining and data analysis were done at UCSD. Kaplan-Meier Survival analysis was performed with Graphpad Prism 5 (GraphPad Software, Inc. La Jolla, CA). Commercial TMA was purchased from US Biomax, Inc. (Cat. No. LV1504). Human NAFLD, NASH12 and NASH34 patients' liver samples were collected at UCSD Medical Center (Table S6). The experimental protocol described in this study was approved by the human subjects institutional review board at UCSD, and all patients provided written informed consent at the initial visit.

Statistical Analyses

Two-tailed Student's t test, one-way ANOVA, χ^2 tests were performed with R (version 3.1.0). $P<0.05$ was considered as statistically significant.

Supplementary Material

Refer to Web version on PubMed Central for supplementary material.

Acknowledgments

We thank Drs. D Brenner, M Karin and other colleagues for advice and reagents. A6 antibody was a generous gift from Factor, VM (NIH). This work was supported by R01CA176012, R01CA188506 and a UCSD-Roche grant to G.S.F.

REFERENCES

Aharoni-Simon M, Hann-Obercyger M, Pen S, Madar Z, Tirosh O. Fatty liver is associated with impaired activity of PPARgamma-coactivator 1alpha (PGC1alpha) and mitochondrial biogenesis in mice. Lab Invest. 2011; 91:1018–1028. [PubMed: 21464822]

Bard-Chapeau EA, Li S, Ding J, Zhang SS, Zhu HH, Princen F, Fang DD, Han T, Bailly-Maitre B, Poli V, et al. Ptpn11/Shp2 acts as a tumor suppressor in hepatocellular carcinogenesis. Cancer Cell. 2011; 19:629–639. [PubMed: 21575863]

Bard-Chapeau EA, Yuan J, Droin N, Long S, Zhang EE, Nguyen TV, Feng GS. Concerted functions of Gab1 and Shp2 in liver regeneration and hepatoprotection. Mol Cell Biol. 2006; 26:4664–4674. [PubMed: 16738330]

Brown PH, Alani R, Preis LH, Szabo E, Birrer MJ. Suppression of oncogene-induced transformation by a deletion mutant of c-jun. Oncogene. 1993; 8:877–886. [PubMed: 8455942]

Cantley LC. The phosphoinositide 3-kinase pathway. Science. 2002; 296:1655–1657. [PubMed: 12040186]

Chalasani N, Younossi Z, Lavine JE, Diehl AM, Brunt EM, Cusi K, Charlton M, Sanyal AJ. The diagnosis and management of non-alcoholic fatty liver disease: practice Guideline by the American Association for the Study of Liver Diseases, American College of Gastroenterology, and the American Gastroenterological Association. Hepatology. 2012; 55:2005–2023. [PubMed: 22488764]

Chalhoub N, Baker SJ. PTEN and the PI3-Kinase Pathway in Cancer. Annual Review of Pathology-Mechanisms of Disease. 2009; 4:127–150.

Chan RJ, Feng GS. PTPN11 is the first identified proto-oncogene that encodes a tyrosine phosphatase. Blood. 2007; 109:862–867. [PubMed: 17053061]

Chen YN, LaMarche MJ, Chan HM, Fekkes P, Garcia-Fortanet J, Acker MG, Antonakos B, Chen CH, Chen Z, Cooke VG, et al. Allosteric inhibition of SHP2 phosphatase inhibits cancers driven by receptor tyrosine kinases. Nature. 2016; 535:148–152. [PubMed: 27362227]

Cross DA, Alessi DR, Cohen P, Andjelkovich M, Hemmings BA. Inhibition of glycogen synthase kinase-3 by insulin mediated by protein kinase B. Nature. 1995; 378:785–789. [PubMed: 8524413]

Eferl R, Wagner EF. AP-1: a double-edged sword in tumorigenesis. Nat Rev Cancer. 2003; 3:859–868. [PubMed: 14668816]

Feng GS. Conflicting roles of molecules in hepatocarcinogenesis: paradigm or paradox. Cancer Cell. 2012; 21:150–154. [PubMed: 22340589]

Galicia VA, He L, Dang H, Kanel G, Vendryes C, French BA, Zeng N, Bayan JA, Ding W, Wang KS, et al. Expansion of hepatic tumor progenitor cells in Pten-null mice requires liver injury and is reversed by loss of AKT2. Gastroenterology. 2010; 139:2170–2182. [PubMed: 20837017]

Gotschel F, Kern C, Lang S, Sparna T, Markmann C, Schwager J, McNelly S, von Weizsacker F, Laufer S, Hecht A, Merfort I. Inhibition of GSK3 differentially modulates NF-kappaB, CREB, AP-1 and beta-catenin signaling in hepatocytes, but fails to promote TNF-alpha-induced apoptosis. Exp Cell Res. 2008; 314:1351–1366. [PubMed: 18261723]

Han T, Xiang DM, Sun W, Liu N, Sun HL, Wen W, Shen WF, Wang RY, Chen C, Wang X, et al. PTPN11/Shp2 Overexpression Enhances Liver Cancer Progression and Predicts Poor Prognosis of Patients. J Hepatol. 2015

He G, Dhar D, Nakagawa H, Font-Burgada J, Ogata H, Jiang Y, Shalapour S, Seki E, Yost SE, Jepsen K, et al. Identification of liver cancer progenitors whose malignant progression depends on autocrine IL-6 signaling. Cell. 2013; 155:384–396. [PubMed: 24120137]

He G, Yu GY, Temkin V, Ogata H, Kuntzen C, Sakurai T, Sieghart W, Peck-Radosavljevic M, Leffert HL, Karin M. Hepatocyte Ikkβeta/NF-kappaB inhibits tumor promotion and progression by

preventing oxidative stress-driven STAT3 activation. Cancer Cell. 2010; 17:286–297. [PubMed: 20227042]

He L, Gubbins J, Peng Z, Medina V, Fei F, Asahina K, Wang J, Kahn M, Rountree CB, Stiles BL. Activation of hepatic stellate cell in Pten null liver injury model. Fibrogenesis Tissue Repair. 2016; 9:8. [PubMed: 27307790]

Horie Y, Suzuki A, Kataoka E, Sasaki T, Hamada K, Sasaki J, Mizuno K, Hasegawa G, Kishimoto H, Iizuka M, et al. Hepatocyte-specific Pten deficiency results in steatohepatitis and hepatocellular carcinomas. J Clin Invest. 2004; 113:1774–1783. [PubMed: 15199412]

Jiang C, Hu F, Tai Y, Du J, Mao B, Yuan Z, Wang Y, Wei L. The tumor suppressor role of Src homology phosphotyrosine phosphatase 2 in hepatocellular carcinoma. J Cancer Res Clin Oncol. 2012; 138:637–646. [PubMed: 22228034]

Kaposi-Novak P, Lee JS, Gomez-Quiroz L, Coulouarn C, Factor VM, Thorgeirsson SS. Met-regulated expression signature defines a subset of human hepatocellular carcinomas with poor prognosis and aggressive phenotype. J Clin Invest. 2006; 116:1582–1595. [PubMed: 16710476]

Kenerson HL, Yeh MM, Kazami M, Jiang X, Riehle KJ, McIntyre RL, Park JO, Kwon S, Campbell JS, Yeung RS. Akt and mTORC1 have different roles during liver tumorigenesis in mice. Gastroenterology. 2013; 144:1055–1065. [PubMed: 23376645]

Lade A, Noon LA, Friedman SL. Contributions of metabolic dysregulation and inflammation to nonalcoholic steatohepatitis, hepatic fibrosis, and cancer. Curr Opin Oncol. 2013; 26:100–107.

Lai, LA., Zhao, C., Zhang, EE., Feng, GS. The Shp-2 tyrosine phosphatase. In: Arino, J., Alexander, D., editors. Protein phosphatases. Berlin Heidelberg: Springer-Verlag; 2004. p. 275-299.

Lanaya H, Natarajan A, Komposch K, Li L, Amberg N, Chen L, Wculek SK, Hammer M, Zenz R, Peck-Radosavljevic M, et al. EGFR has a tumour-promoting role in liver macrophages during hepatocellular carcinoma formation. Nat Cell Biol. 2014; 16:972–981. 971–977. [PubMed: 25173978]

Lesche R, Groszer M, Gao J, Wang Y, Messing A, Sun H, Liu X, Wu H. Cre/loxP-mediated inactivation of the murine Pten tumor suppressor gene. Genesis. 2002; 32:148–149. [PubMed: 11857804]

Li J, Chen H, Tang MS, Shi X, Amin S, Desai D, Costa M, Huang C. PI-3K and Akt are mediators of AP-1 induction by 5-MCDE in mouse epidermal Cl41 cells. J Cell Biol. 2004; 165:77–86. [PubMed: 15067018]

Li S, Hsu DD, Li B, Luo X, Alderson N, Qiao L, Ma L, Zhu HH, He Z, Suino-Powell K, et al. Cytoplasmic tyrosine phosphatase Shp2 coordinates hepatic regulation of bile acid and FGF15/19 signaling to repress bile acid synthesis. Cell Metab. 2014; 20:320–332. [PubMed: 24981838]

Liao R, Sun TW, Yi Y, Wu H, Li YW, Wang JX, Zhou J, Shi YH, Cheng YF, Qiu SJ, Fan J. Expression of TREM-1 in hepatic stellate cells and prognostic value in hepatitis B-related hepatocellular carcinoma. Cancer Sci. 2012; 103:984–992. [PubMed: 22417086]

Llovet JM, Ricci S, Mazzaferro V, Hilgard P, Gane E, Blanc JF, de Oliveira AC, Santoro A, Raoul JL, Forner A, et al. Sorafenib in advanced hepatocellular carcinoma. N Engl J Med. 2008; 359:378–390. [PubMed: 18650514]

Maeda S, Kamata H, Luo JL, Leffert H, Karin M. Ikkβeta couples hepatocyte death to cytokine-driven compensatory proliferation that promotes chemical hepatocarcinogenesis. Cell. 2005; 121:977–990. [PubMed: 15989949]

Michelotti GA, Machado MV, Diehl AM. NAFLD, NASH and liver cancer. Nat Rev Gastroenterol Hepatol. 2013; 10:656–665. [PubMed: 24080776]

Min L, Ji Y, Bakiri L, Qiu Z, Cen J, Chen X, Chen L, Scheuch H, Zheng H, Qin L, et al. Liver cancer initiation is controlled by AP-1 through SIRT6-dependent inhibition of survivin. Nat Cell Biol. 2012; 14:1203–1211. [PubMed: 23041974]

Nakagawa H, Umemura A, Taniguchi K, Font-Burgada J, Dhar D, Ogata H, Zhong Z, Valasek MA, Seki E, Hidalgo J, et al. ER stress cooperates with hypernutrition to trigger TNF-dependent spontaneous HCC development. Cancer Cell. 2014; 26:331–343. [PubMed: 25132496]

Neel BG, Gu H, Pao L. The 'Shp'ing news: SH2 domain-containing tyrosine phosphatases in cell signaling. Trends Biochem Sci. 2003; 28:284–293. [PubMed: 12826400]

Park EJ, Lee JH, Yu GY, He G, Ali SR, Holzer RG, Osterreicher CH, Takahashi H, Karin M. Dietary and genetic obesity promote liver inflammation and tumorigenesis by enhancing IL-6 and TNF expression. Cell. 2010; 140:197–208. [PubMed: 20141834]

Peloponese JM Jr, Jeang KT. Role for Akt/protein kinase B and activator protein-1 in cellular proliferation induced by the human T-cell leukemia virus type 1 tax oncoprotein. J Biol Chem. 2006; 281:8927–8938. [PubMed: 16436385]

Pilati C, Letouze E, Nault JC, Imbeaud S, Boulai A, Calderaro J, Poussin K, Franconi A, Couchy G, Morcrette G, et al. Genomic profiling of hepatocellular adenomas reveals recurrent FRK-activating mutations and the mechanisms of malignant transformation. Cancer Cell. 2014; 25:428–441. [PubMed: 24735922]

Ransone LJ, Verma IM. Nuclear proto-oncogenes fos and jun. Annu Rev Cell Biol. 1990; 6:539–557. [PubMed: 2125830]

Sanchez-Pareja A, Clement S, Peyrou M, Spahr L, Negro F, Rubbia-Brandt L, Foti M. Phosphatase and tensin homolog is a differential diagnostic marker between nonalcoholic and alcoholic fatty liver disease. World J Gastroenterol. 2016; 22:3735–3745. [PubMed: 27076758]

Shi ZQ, Lu W, Feng GS. The Shp-2 tyrosine phosphatase has opposite effects in mediating the activation of extracellular signal-regulated and c-Jun NH2-terminal mitogen-activated protein kinases. J Biol Chem. 1998; 273:4904–4908. [PubMed: 9478933]

Shimizu Y, Kinoshita I, Kikuchi J, Yamazaki K, Nishimura M, Birrer MJ, Dosaka-Akita H. Growth inhibition of non-small cell lung cancer cells by AP-1 blockade using a cJun dominant-negative mutant. Br J Cancer. 2008; 98:915–922. [PubMed: 18283312]

Song MS, Salmena L, Pandolfi PP. The functions and regulation of the PTEN tumour suppressor. Nature Reviews Molecular Cell Biology. 2012

Stiles B, Wang Y, Stahl A, Bassilian S, Lee WP, Kim YJ, Sherwin R, Devaskar S, Lesche R, Magnuson MA, Wu H. Liver-specific deletion of negative regulator Pten results in fatty liver and insulin hypersensitivity [corrected]. Proc Natl Acad Sci U S A. 2004; 101:2082–2087. [PubMed: 14769918]

Takami T, Kaposi-Novak P, Uchida K, Gomez-Quiroz LE, Conner EA, Factor VM, Thorgeirsson SS. Loss of hepatocyte growth factor/c-Met signaling pathway accelerates early stages of N-nitrosodiethylamine induced hepatocarcinogenesis. Cancer Res. 2007; 67:9844–9851. [PubMed: 17942915]

Theise ND. World Cancer Report 2014: IARC). 2014

Wang Q, Yu WN, Chen X, Peng XD, Jeon SM, Birnbaum MJ, Guzman G, Hay N. Spontaneous Hepatocellular Carcinoma after the Combined Deletion of Akt Isoforms. Cancer Cell. 2016; 29:523–535. [PubMed: 26996309]

Wolf MJ, Adili A, Piotrowitz K, Abdullah Z, Boege Y, Stemmer K, Ringelhan M, Simonavicius N, Egger M, Wohlleber D, et al. Metabolic activation of intrahepatic CD8+ T cells and NKT cells causes nonalcoholic steatohepatitis and liver cancer via cross-talk with hepatocytes. Cancer Cell. 2014; 26:549–564. [PubMed: 25314080]

Worby CA, Dixon JE. Pten. Annu Rev Biochem. 2014; 83:641–669. [PubMed: 24905788]

Yoshida LS, Miyazawa T, Hatayama I, Sato K, Fujimoto K, Kaneda T. Phosphatidylcholine peroxidation and liver cancer in mice fed a choline-deficient diet with ethionine. Free Radic Biol Med. 1993; 14:191–199. [PubMed: 8425721]

Zhang EE, Chapeau E, Hagihara K, Feng GS. Neuronal Shp2 tyrosine phosphatase controls energy balance and metabolism. Proc Natl Acad Sci U S A. 2004; 101:16064–16069. [PubMed: 15520383]

Zhang XF, Tan X, Zeng G, Misse A, Singh S, Kim Y, Klaunig JE, Monga SP. Conditional beta-catenin loss in mice promotes chemical hepatocarcinogenesis: role of oxidative stress and platelet-derived growth factor receptor alpha/phosphoinositide 3-kinase signaling. Hepatology. 2010; 52:954–965. [PubMed: 20583210]

Zhu HH, Luo X, Zhang K, Cui J, Zhao H, Ji Z, Zhou Z, Yao J, Zeng L, Ji K, et al. Shp2 and Pten have antagonistic roles in myeloproliferation but cooperate to promote erythropoiesis in mammals. Proceedings of the National Academy of Sciences. 2015

Zhu X, Jiang S, Hu N, Luo F, Dong H, Kang YM, Jones KR, Zou Y, Xiong L, Ren J. Tumour necrosis factor-alpha inhibition with lenalidomide alleviates tissue oxidative injury and apoptosis in ob/ob obese mice. Clin Exp Pharmacol Physiol. 2014; 41:489–501. [PubMed: 24739012]

Zucman-Rossi J, Villanueva A, Nault JC, Llovet JM. Genetic Landscape and Biomarkers of Hepatocellular Carcinoma. Gastroenterology. 2015; 149:1226–1239. e1224. [PubMed: 26099527]

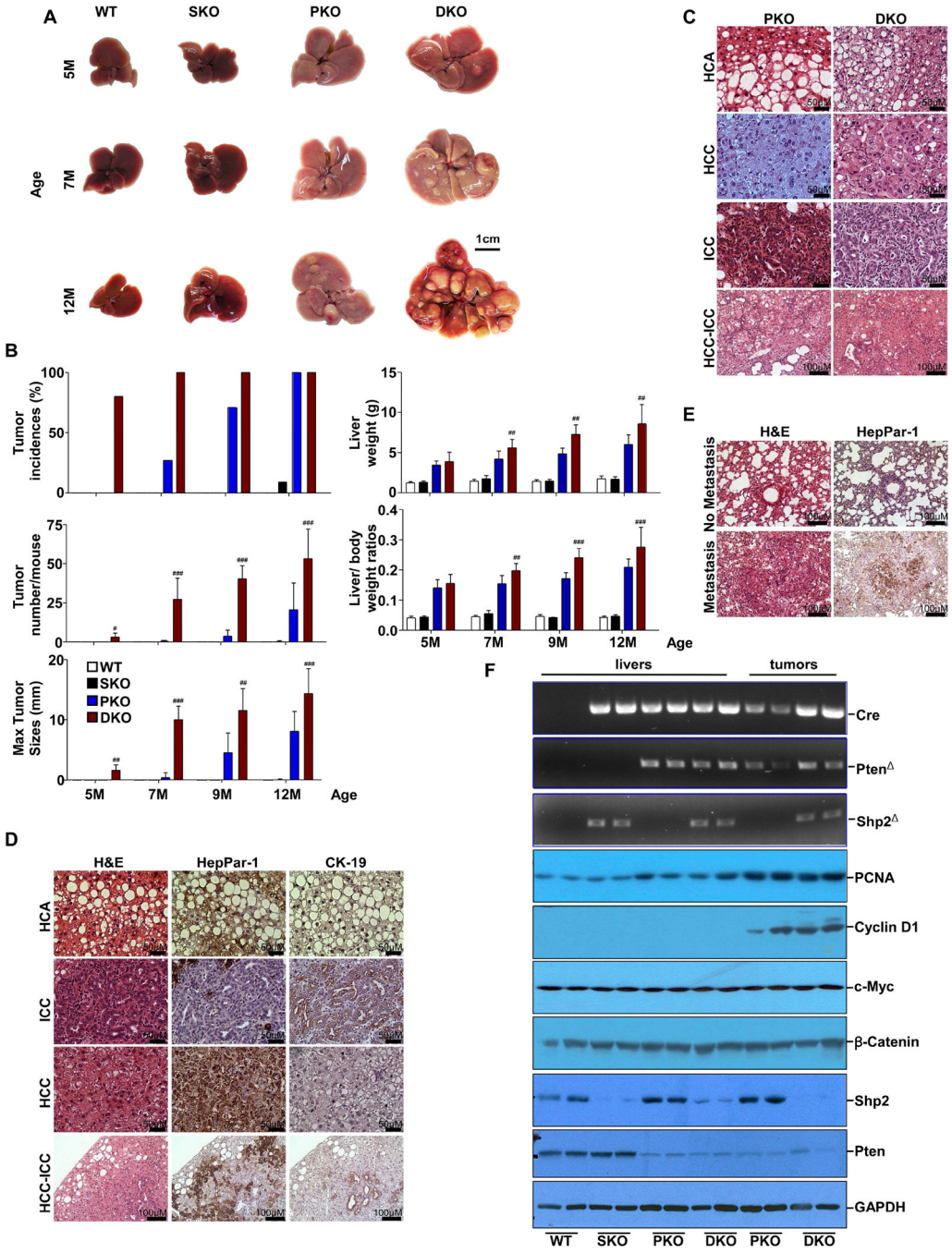

Figure 1. Shp2 and Pten Cooperate to Suppress Liver Tumorigenesis

(A) Representative macroscopic view of livers.

(B) Tumor incidences, maximal tumor diameters, tumor number /mouse, liver weight and liver/ body weight (BW) ratios were compared (n=5–19). Data are represented as mean±SD. #, $p<0.05$; ##, $p<0.01$; and ###, $p<0.001$, for *DKO. vs. PKO*. p-value <0.001 in all comparison for *PKO. vs. WT*. p-value <0.001 in all comparison for *DKO. vs. WT* or *DKO .vs. SKO*.

(C) Representative H&E staining of hepatocellular adenoma (HCA), hepatocellular carcinoma (HCC), intrahepatic cholangiocarcinoma (ICC), and mixed HCC-ICC tumors.
(D) Representative H&E and immunostaining of tumor sections from *DKO* mice.
(E) H&E and immunostaining of lung sections from *DKO* mice.
(F) PCR analysis (upper) of genomic DNAs with *Shp2* deletion ($Shp2^{\Delta}$), *Pten* deletion ($Pten^{\Delta}$) and *Cre*, and immunoblot analysis (lower) of expression of cell cycle-related genes, oncogenes, *Shp2* and *Pten* in liver tissues or tumors from the 4 groups of mice. See also Table S1.

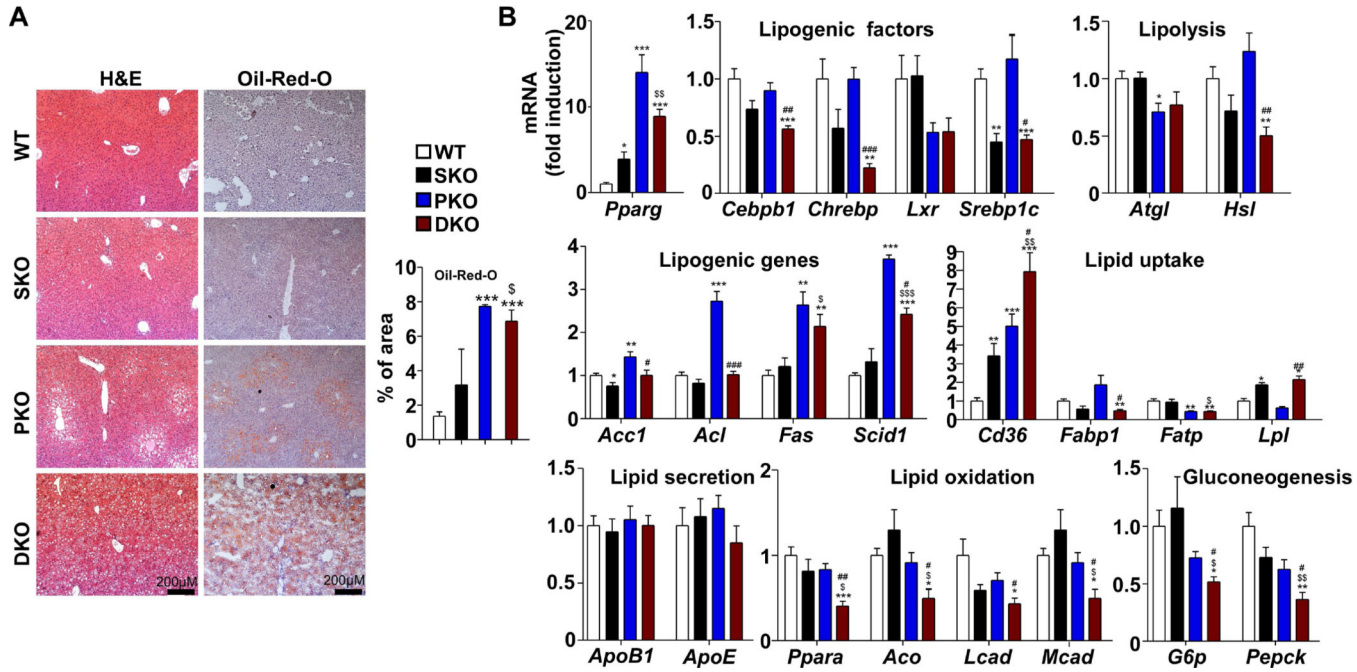

Figure 2. Dual deletion of *Shp2* and *Pten* in Hepatocytes Promotes Hepatic Steatosis

(A) Left, representative H&E and Oil-Red-O staining of liver sections. Right, quantification of percentage of positive Oil-Red-O staining area (n=3).

(B) mRNA levels of key genes in lipid metabolism and gluconeogenesis were determined with qRT-PCR and compared (n=5).

All samples used in this figure were obtained from 2-month-old mice. Data are shown as means ± S.D. *, **, or *** indicates *SKO*. *PKO* or *DKO* vs. *WT*. $, $$, or $$$ indicates *DKO* vs. *SKO*. #, ## or ### indicates *DKO* vs. *PKO*. *, $ or # indicates $p<0.05$. **, $$ or ## indicates $p<0.01$. ***, $$$ or ### indicates $p<0.001$. See also Figure S1.

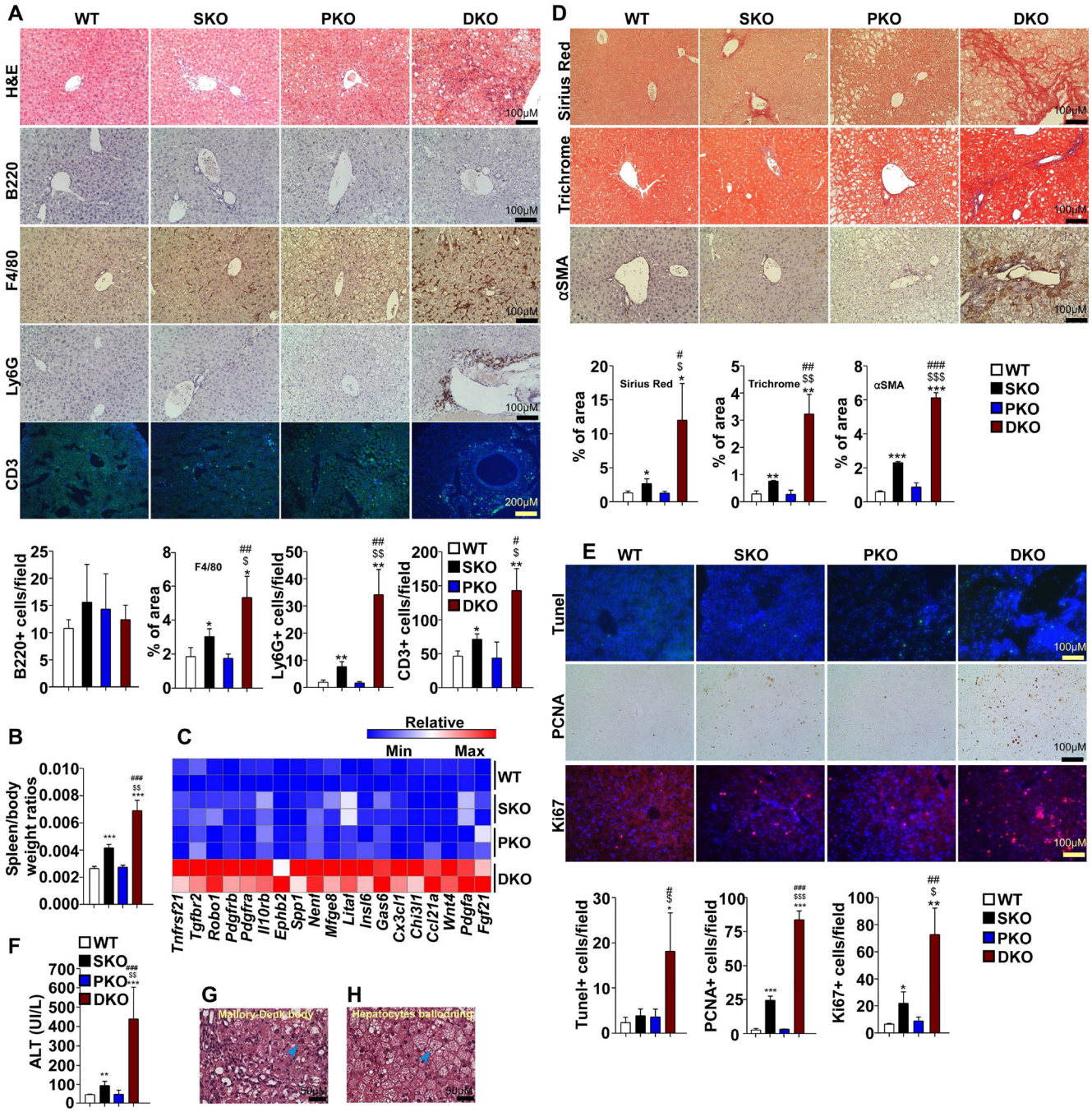

Figure 3. *DKO* mice Develop Early-Onset NASH

(A) Top, representative H&E and immunostaining of immune cells in the livers. Bottom, quantification of B220, Ly6G, CD3 positive cells and percentage of positive F4/80 staining area (n=3).

(B) Spleen/body weight ratios were compared (n=6).

(C) Heatmap with liver cDNA microarray data shows mRNA levels of secretory factors and related receptors with color intensity. Each row indicates one mouse. Color scale is provided as reference.

(D) Top, Picro-Sirius Red, Masson's Trichrome and αSMA immunostaining of liver sections. Bottom, quantification of percentage of positive Sirius Red, Trichrome and α-SMA staining area (n=3).
(E) Top, Tunel assay, Ki67 and PCNA immunostaining of liver sections. Bottom, quantification of Tunel, Ki67 or PCNA positive hepatocytes (n=3 to 6).
(F) Serum ALT was measured and compared (n=6).
(G, H) Representative H&E staining shows Mallory-Denk body and ballooning hepatocytes (arrowhead) in *DKO* liver.
All samples used in this figure were obtained from 2-month-old mice. Data are shown as means ± S.D. *, **, or *** indicates *SKO*, *PKO* or *DKO* vs. *WT*. $, $$or $$$ indicates *DKO* vs. *SKO*. # or ### indicates *DKO* vs. *PKO**, $ or # indicates $p<0.05$. ** or $$ indicates $p<0.01$. ***, $$$ or ### indicates $p<0.001$
See also Figure S2.

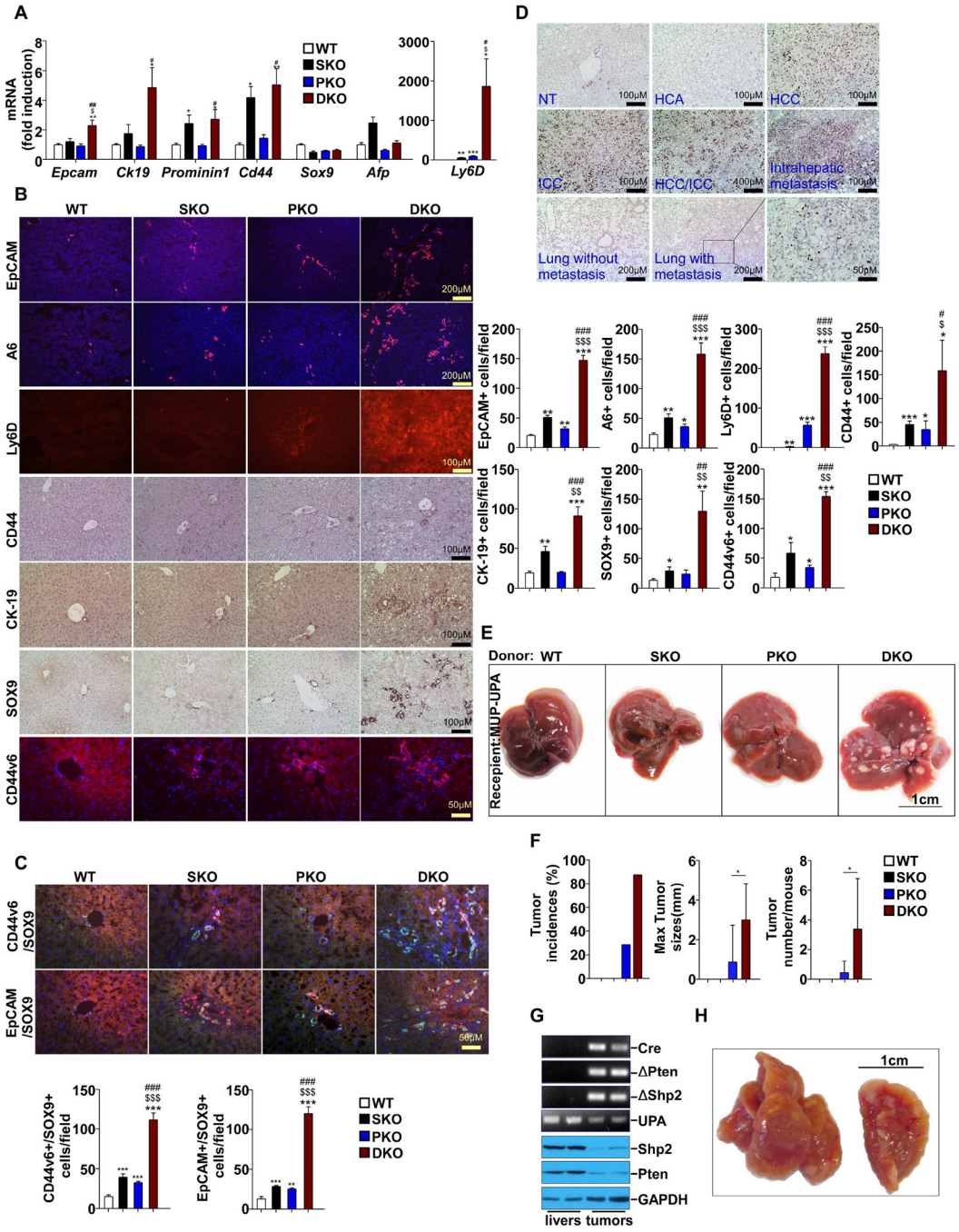

Figure 4. Early Expansion of Liver Tumor Initiating Cells (TICs) in *DKO* Mice

(A) mRNA levels of TIC markers were determined with qPCR and compared among 2-month-old *WT* mice (n=5).

(B) Left, representative immunostaining of TIC markers on liver sections from 2-month-old mice. Right, quantification of EpCAM, A6, Ly6D, CD44, CK-19, SOX9 and CD44v6 positive cells (n=3).

(C) Top, representative co-immunostaining of CD44v6/SOX9 and EpCAM/SOX9 on liver sections from 2-month-old mice. Bottom, quantification of CD44v6/SOX9 and EpCAM/SOX9 positive cells (n=3).
(D) Representative SOX9 immunostaining of sections from 12-month-old *DKO* mice. (E–J) Data from *MUP-UPA* mice 5 months after transplantation with *DKO* hepatocytes
(E) Macroscopic view of representative livers from *MUP-uPA* mice 5 months after transplantion with hepatocytes from 2- to 3-month-old *WT*, *SKO*, *PKO* and *DKO*.
(F) Tumor incidences, sizes (maximal tumor diameters), and tumor numbers/mouse were compared (n=7~9). Data are represented as mean±SD.
(G) PCR analysis (upper) of genomic DNA and immunoblot analysis (lower) of lysates from respective liver or tumor tissues.
(H) Macroscopic view of a representative lung with metastases.
Data are shown as means ± S.D. *, **, or *** indicates *SKO*, *PKO* or *DKO* vs. *WT*. $ indicates *DKO* vs. *SKO*. # or ## indicates *DKO* vs. *PKO**, $ or # indicates $p<0.05$. ** or ## indicates $p<0.01$. *** indicates $p<0.001$. See also Figure S3.

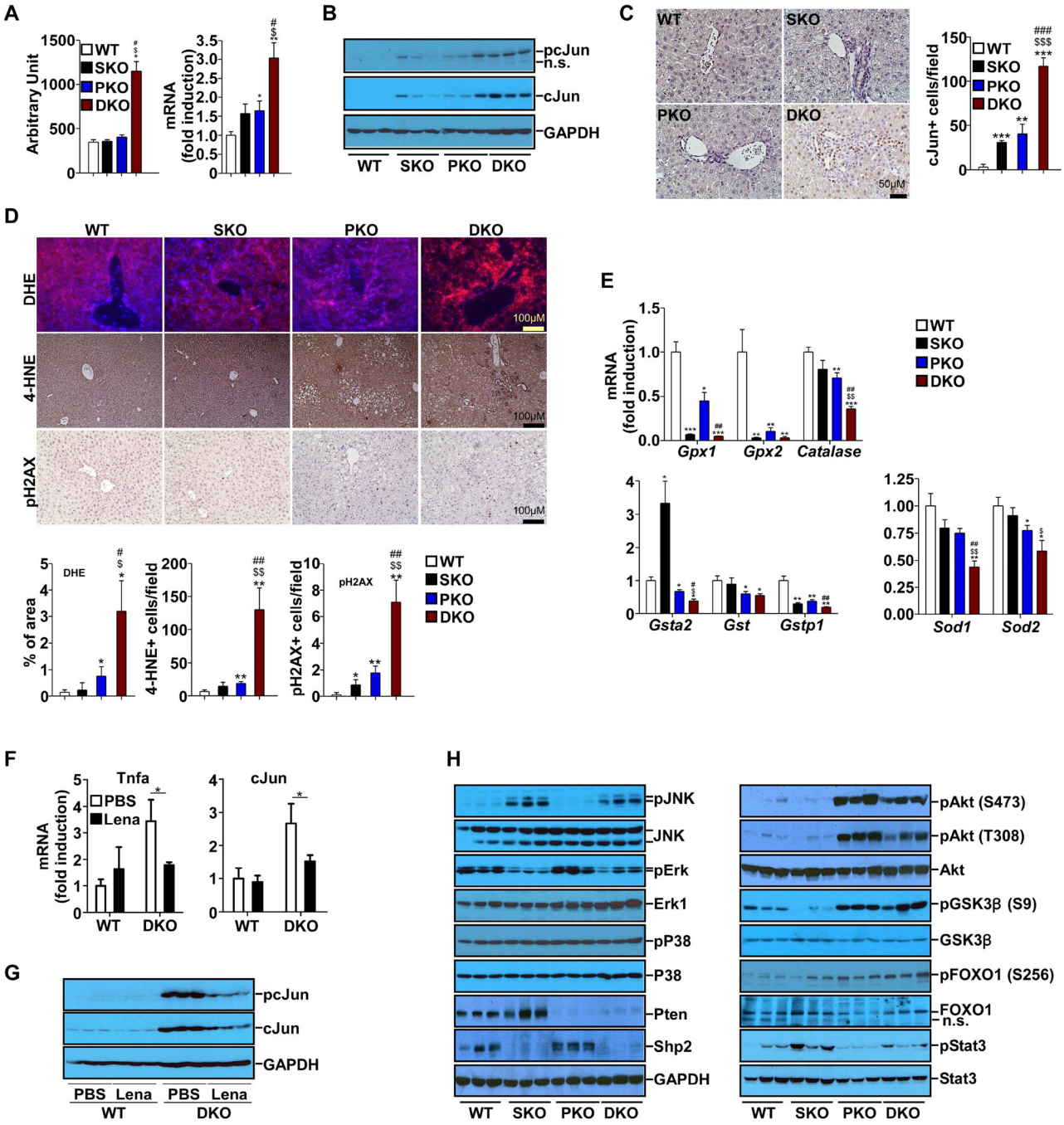

Figure 5. Elevated Expression and Activation of cJun in *DKO* Liver

(A) mRNA levels of *cJun* were determined by cDNA microarray (left) and qPCR(right) (n=5).

(B) Protein and phosphorylation levels of cJun were determined by immunoblot.

(C) Left, cJun immunostaining of liver sections. Right, quantification of cJun positive cells (n=3).

(D) Top, DHE and immunostaining for 4-HNE and pH2AX were performed on liver sections. Bottom, quantification of 4-HNE, pH2AX positive cells and percentage of positive DHE staining area (n=3).
(E) mRNA levels of key genes in reactive oxygen species (ROS) scavenging were determined by qPCR (n=5).
(F) mRNA levels of TNFα and cJun were determined by qPCR (n=4). Data are shown as means ± S.D. * indicates $p<0.05$. (Lena: Lenalidomide)
(G) Protein and phosphorylation levels of cJun were determined by immunoblot (H) Analysis of signaling pathways with immunoblotting of liver lysates.
All samples used in A to E&H were from 2-month-old mice. Data are shown as means ± S.D. *, **, or *** indicates *SKO*, *PKO* or *DKO* vs. *WT*. $ or $$ indicates *DKO* vs. *SKO*. # or ## indicates *DKO* vs. *PKO**, $ or # indicates $p<0.05$. **, $$ or ## indicates $p<0.01$. *** indicates $p<0.001$.
See also Figure S4.

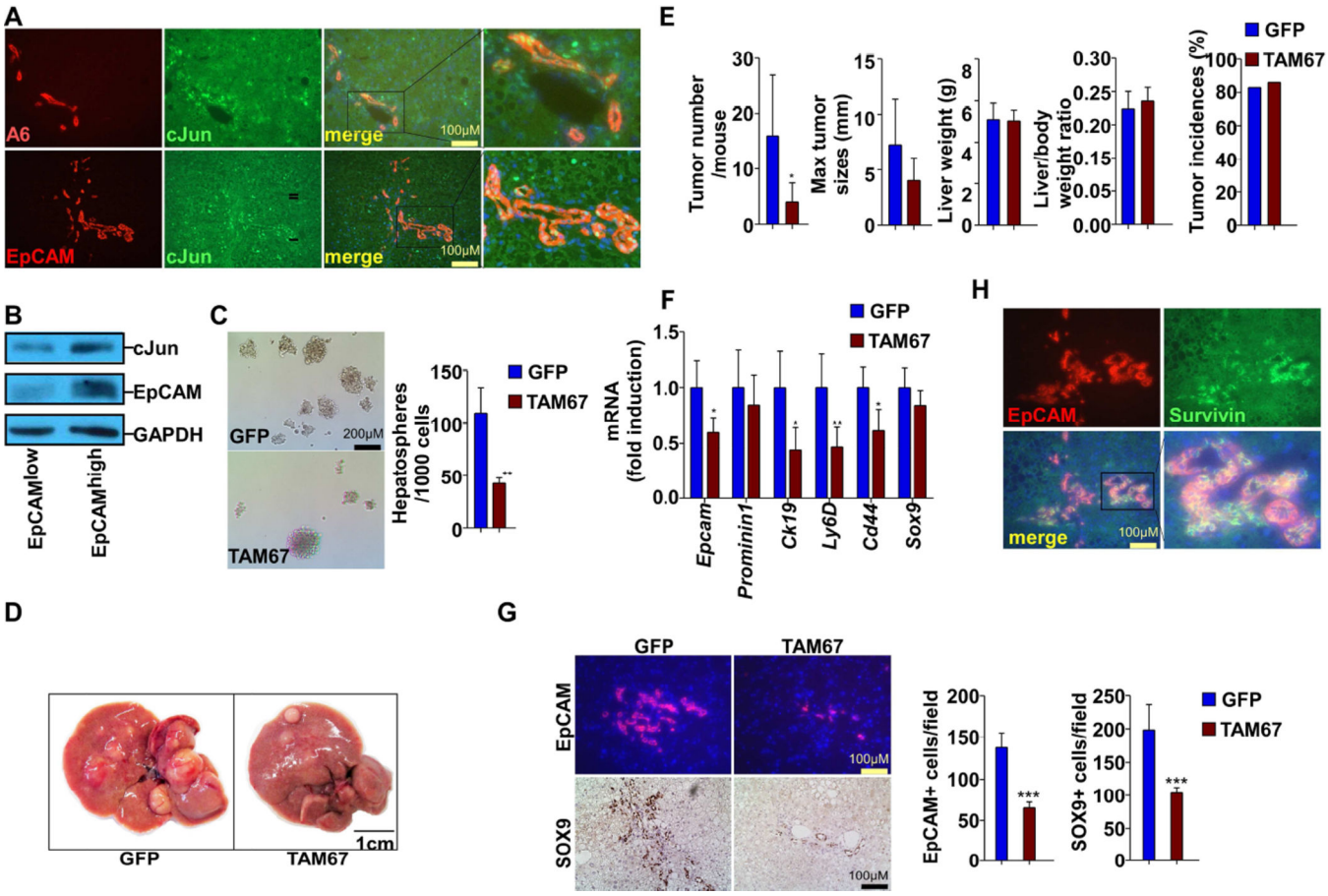

Figure 6. cJUN is Critical for TIC Expansion and Tumorigenesis in *DKO* mice

(A) Co-immunostaining for A6/cJun, EpCAM/cJun on liver sections from 2-month-old *DKO* mice.

(B) HepG2 cells were FACS sorted for EpCAM expression. cJun and EpCAM protein levels were determined by immunoblotting.

(C) Microscopic view of representative hepatospheres formed by HepG2 cells infected with AAV-GFP or AAV-TAM67. Bar chart shows the quantification of hepatospheres/1000 cells. Experiment was performed three times with three wells/group each time.

(D) Macroscopic view of representative livers from *DKO* infected with AAV-GFP or AAV-TAM67.

(E) Tumor number/mouse, maximal tumor diameters, liver weight, liver/body weight (BW) ratios and tumor incidences were determined and compared between mice infected with AAV-GFP or AAV-TAM67 (n = 6~7).

(F) mRNA levels of TIC markers were determined by qPCR and compared between mice infected with AAV-GFP or AAV-TAM67 (n = 5).

(G) Left, immunostaining for EpCAM and SOX9 was performed on liver sections from mice infected with AAV-GFP or AAV-TAM67. Right, quantification of SOX9 and EpCAM positive cells(n=6~7).

(H) Co-immunostaining for EpCAM and Survivin was performed on DKO liver sections. Data are presented as Mean±SD. (*p<0.05,** p<0.01,*** p<0.001) See also Figure S5 and Table S2.

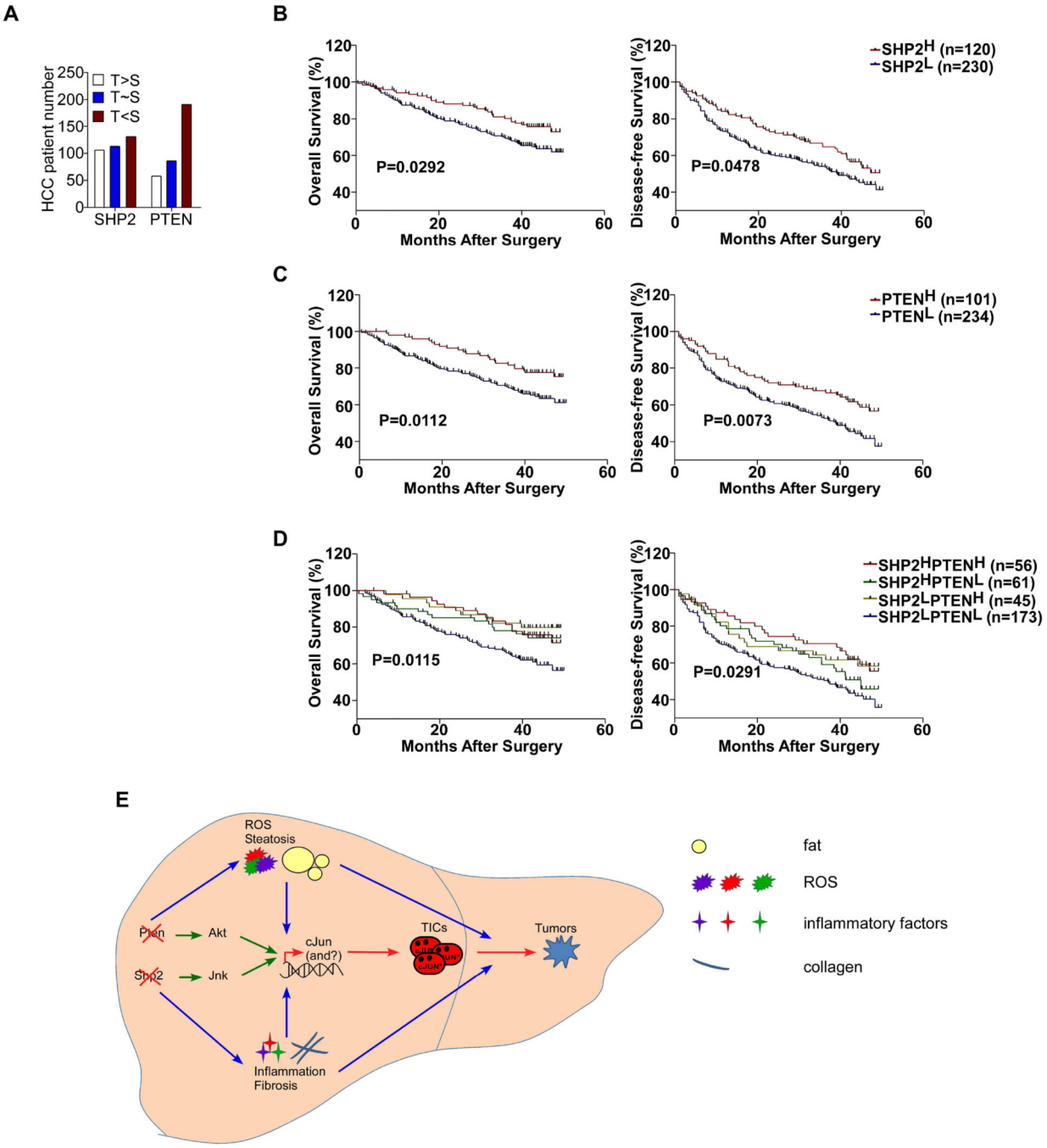

Figure 7. SHP2 and PTEN Deficiencies in Human HCCs

(A) Expression of SHP2 and PTEN was analyzed by immunostaining and compared in 350 pairs of human HCC and tumor-surrounding tissue samples (T: Tumor; S: tumor-surrounding tissue).

(B–D) Kaplan-Meier survival curves of overall survival (left) and disease-free survival (right) based on SHP2 and/or PTEN expression levels in HCC tissues. Samples were grouped by low (score<=1) or high (score>1) expression of each protein. Log-rank test was performed and p values are shown. (E) A model for enhanced liver tumorigenesis driven by

combined deletion of Pten and Shp2. Pten loss leads to Akt over-activation and Shp2 deficiency promotes Jnk upregulation, resulting in increased cJun expression and activation. Ablating Pten and Shp2 also leads to elevated ROS, inflammation, and steatohepatitis etc., driving earlier genesis of TICs and enhanced HCC development.
See also Figure S6–7 and Table S3–6.